ACADEMIC PRESS

Available online at www.sciencedirect.com

SCIENCE DIRECT®

Journal of Sound and Vibration 264 (2003) 453–473

JOURNAL OF SOUND AND VIBRATION

www.elsevier.com/locate/jsvi

Vibration characteristics of piezoelectric torsional transducers

Jin O. Kim[a,*], Oh Soo Kwon[b]

[a] *Department of Mechanical Engineering, Soongsil University, 1–1 Sangdo-dong, Dongjak-gu, Seoul 156-743, South Korea*
[b] *C & C Peripheral Acoustic System Division, Samsung Electro-Mechanics Co., Ltd., 314 Maetan-3dong, Paldal-gu, Suwon, Kyunggi-do 442-743, South Korea*

Received 19 February 2002; accepted 29 July 2002

Abstract

The vibrational characteristics of Langevin–type torsional transducers, which consist of two piezoelectric torsional disks and two elastic blocks, are studied theoretically and experimentally in this paper. The differential equations of piezoelectric torsional motions are derived in terms of the circumferential displacement and the electric potential. Solutions of the boundary-value problem yield the natural frequencies and mode shapes of the transducers, and the natural frequencies are verified by comparing the numerical results with the experimental ones. The theoretical results enable one to quantitatively predict the effect of the elastic blocks on the reduction of the natural frequencies of a Langevin-type torsional transducer.

1. Introduction

Piezoelectric transducers convert electric signals into mechanical vibrations and vice versa [1,2]. A bolt-clamped Langevin-type transducer, referred to as BLT hereafter, is one of the piezoelectric transducers. A BLT consists of piezoelectric disks and two elastic blocks clamped at each end as shown in Fig. 1, and efficiently generates mechanical vibrations of desired frequencies [3]. A BLT plays the role of an actuator in several applications. Most of them use longitudinal vibrations in the thickness direction of piezoelectric disks. In contrast, this paper is concerned with the transducers generating torsional vibrations in an elastic rod, which is supposed to work as a viscosity sensor [4,5].

The torsional transducers must be more complicated to make than longitudinal transducers. It was suggested to make a torsional transducer disk either by assembling several pieces of polarized

*Corresponding author.
E-mail address: jokim@ssu.ac.kr (J.O. Kim).

0022-460X/03/$ - see front matter
doi:10.1016/S0022-460X(02)01234-8

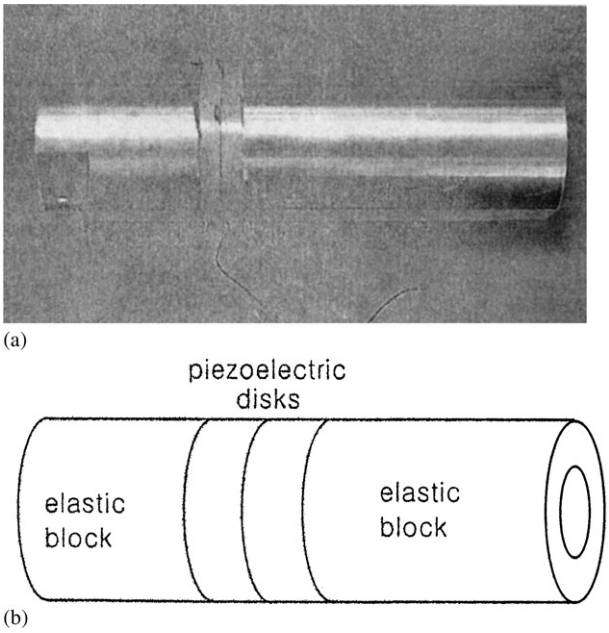

Fig. 1. Langevin-type transducer, consisting of two piezoelectric disks and two elastic blocks: (a) photo, (b) schematic diagram.

cubes [6] or by alternately polarizing the even number of sectors of a disk and covering it with alternate electrodes [7]. Another scheme, suggested earlier [8], is to circumferentially polarize a disk. This means appears to be more convenient to execute and more reliable. The torsional disks considered in this paper have been fabricated by following this scheme.

The piezoelectric torsional disks composing the BLT shown in Fig. 1 have been fabricated according to the process illustrated in Fig. 2. (a) A disk molded with ceramic powder is divided into an even number (16 in this paper) of sectors, and the alternate sectors are painted with silver electrodes (shadowed area in the figure). (b) A couple of adjacent electrodes are driven by electric voltage, and one area is polarized in the circumferential direction. (c) Polarizing is continued in the remaining areas of the disk. (d) The divided electrodes are removed after polarization. (e) Other electrodes are painted on the top and bottom surfaces of the disk. (f) The electrodes are connected to a driving circuit.

The torsional disks are usually of high-frequency resonance, and they are assembled with two elastic blocks to lower the resonance frequency. The disks and blocks are clamped together with a bolt. This kind of transducer is called a torsional BLT, and Fig. 1 shows its typical shape. A study on the similar type torsional transducer was reported before [9], but it suggested a theoretical approach without verifying the result and showed a derivation of the electromechanical equivalent circuit.

This paper deals with a theoretical and experimental study on the vibration characteristics of the piezoelectric torsional disks and torsional BLTs. The differential equations and boundary conditions of piezoelectric torsional motion are formulated in terms of the circumferential

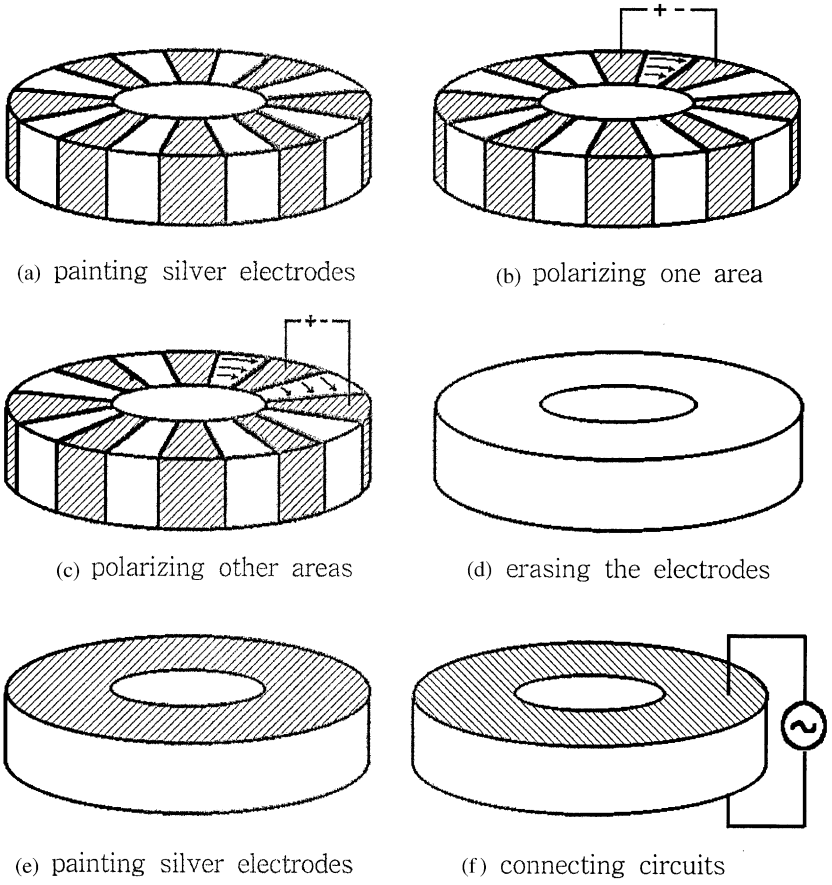

Fig. 2. Fabrication process of a piezoelectric torsional disk. (a) painting silver electrodes, (b) polarizing one area, (c) polarizing other areas, (d) erasing the electrodes, (e) painting silver electrodes, (f) connecting circuits.

displacement and the electric potential. For the torsional disks and then for the torsional BLTs, the boundary-value problems are solved to yield the natural frequencies and mode shapes. The theoretical solutions are then compared with experimental observations in the sense of the natural frequency.

2. Formulation of the electromechanical problem

The electromechanical relations were well formulated for the longitudinal vibrations in the thickness direction of a piezoelectric disk [10]. Torsional vibrations in a cylindrical piezoelectric material can also be described in terms of the circumferential displacement $u(r, z, t)$ and electric potential $\phi(r, z, t)$. The shear stress $\tau_{z\theta}$ in the circumferential direction and the electric displacement D on a circular (or an annular) cross-section have the constitutive relations with the

shear strain ($\partial u/\partial z$) and the electric field ($-\partial\phi/\partial z$) as follows:

$$\tau_{z\theta} = G\frac{\partial u}{\partial z} + \varepsilon\frac{\partial \phi}{\partial z}, \tag{1}$$

$$D = \varepsilon\frac{\partial u}{\partial z} - \zeta\frac{\partial \phi}{\partial z}, \tag{2}$$

where G is the shear modulus, ε is the piezoelectric stress constant, and ζ is the permittivity.

The equation of motion derived from the force equilibrium is

$$\frac{\partial \tau_{z\theta}}{\partial z} = \rho\frac{\partial^2 u}{\partial t^2} \tag{3}$$

and the electrostatic equation is

$$\frac{\partial D}{\partial z} = 0, \tag{4}$$

where ρ is the mass density. Inserting Eqs. (1) and (2) into Eqs. (3) and (4) yields the following governing equations:

$$\frac{\partial^2 u}{\partial z^2} = \frac{1}{c^2}\frac{\partial^2 u}{\partial t^2}, \tag{5}$$

$$\frac{\partial^2 \phi}{\partial z^2} = \frac{\varepsilon}{\zeta}\frac{\partial^2 u}{\partial z^2}, \tag{6}$$

where $c(=[\hat{G}/\rho]^{1/2})$ in the wave Eq. (5) is the propagation speed of the torsional wave, and $\hat{G}(=G+\varepsilon^2/\zeta)$ is the modified shear modulus including the piezoelectric phenomenon.

When the voltage applied to the electrodes is a harmonic function of time t with frequency ω, the displacement u and the electric potential ϕ are regarded as harmonic functions of time with the same frequency. Moreover, Eqs. (5) and (6) are independent of the radial co-ordinate r. Therefore, $u(r,z,t)$ and $\phi(r,z,t)$ can be expressed through the separation of variables as seen in the following:

$$u(r,z,t) = \tilde{u}(z)R(r)\mathrm{e}^{\mathrm{j}\omega t}, \tag{7}$$

$$\phi(r,z,t) = \tilde{\phi}(z)R(r)\mathrm{e}^{\mathrm{j}\omega t}. \tag{8}$$

Here $R(r)$ is an arbitrary function of the radial co-ordinate r, but it is linearly proportional to r in the fundamental mode. Substituting Eqs. (7) and (8) into Eqs. (5) and (6) provides the following governing equations in terms of $\tilde{u}(z)$ and $\tilde{\phi}(z)$:

$$\frac{\mathrm{d}^2\tilde{u}}{\mathrm{d}z^2} + k^2\tilde{u} = 0, \tag{9}$$

$$\frac{\mathrm{d}^2\tilde{\phi}}{\mathrm{d}z^2} = \frac{\varepsilon}{\zeta}\frac{\mathrm{d}^2\tilde{u}}{\mathrm{d}z^2}, \tag{10}$$

where $k(=\omega/c)$ is the wavenumber.

The solution of the Helmholtz equation (9) has the following form:

$$\tilde{u}(z) = A\cos kz + B\sin kz. \tag{11}$$

After inserting Eq. (11) into Eq. (10), the solution of $\tilde{\phi}(z)$ is obtained as follows:

$$\tilde{\phi}(z) = \frac{\varepsilon}{\zeta}(A \cos kz + B \sin kz) + az + b. \tag{12}$$

The unknown constants A, B, a, and b are determined according to the boundary conditions.

In addition, the electric displacement $D(r, z, t)$ is also expressed through the separation of variables seen in the following:

$$D(r, z, t) = \tilde{D}(z)R(r)e^{j\omega t}. \tag{13}$$

Inserting Eqs. (7), (8), and (13) into Eq. (2) and rearranging the equation yields the following:

$$\tilde{D}(z) = \varepsilon\frac{d\tilde{u}}{dz} - \zeta\frac{d\tilde{\phi}}{dz}. \tag{14}$$

Substituting Eqs. (11) and (12) into Eq. (14) simplifies the equation as follows:

$$\tilde{D} = -\zeta a = constant. \tag{15}$$

Eq. (15) means that the electric displacement $D(r, z, t)$ is uniform along the thickness direction of the disk.

3. Vibration of single-disk transducers

Since a BLT consists of piezoelectric disks and elastic blocks as shown in Fig. 1, it is needed to first clarify the vibration characteristics of the disks. The unknown constants in solutions (11) and (12) can be determined by applying mechanical and electrical boundary conditions.

3.1. Analysis

A schematic diagram of a torsional transducer of a single disk is shown in Fig. 3. The piezoelectric transducer has the thickness l and is driven by the electric voltage $V_0e^{j\omega t}$ applied to its side surfaces.

For the transducer fixed at one side ($z = 0$) and free at the other side ($z = l$), the boundary conditions are the following:

$$\tilde{u} = 0 \quad \text{and} \quad \tilde{\phi} = 0 \qquad \text{at } z = 0, \tag{16a, b}$$

$$\tilde{\tau} = 0 \quad \text{and} \quad \tilde{\phi} = V_0 \qquad \text{at } z = l. \tag{16c, d}$$

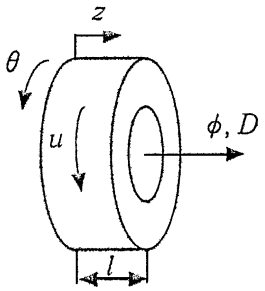

Fig. 3. Schematic diagram of a single-disk transducer.

After using the shear stress $\tau_{z\theta}(=\tilde{\tau}(z)R(r)e^{j\omega t})$ expressed in Eq. (1) and the boundary conditions (16), the unknown constants of Eqs. (11) and (12) are determined and the solutions of Eqs. (5) and (6) are obtained in the following manner:

$$\tilde{u}(z) = \frac{\varepsilon V_0}{\Delta_1} \sin kz, \tag{17}$$

$$\tilde{\phi}(z) = \frac{V_0}{\Delta_1}\left[\frac{\varepsilon^2}{\zeta} \sin kz - (\hat{G}k \cos kl\ )z\right], \tag{18}$$

$$\tilde{D} = \frac{\zeta V_0}{\Delta_1} \hat{G}k \cos kl, \tag{19}$$

where

$$\Delta_1 \equiv \frac{\varepsilon^2}{\zeta} \sin kl - \hat{G}kl \cos kl = 0 \tag{20}$$

is the characteristic equation representing the resonance of the single–disk torsional transducer fixed at one side and free at the other. Here, $\varepsilon^2/\hat{G}\zeta$ is the square of electromechanical coupling coefficient (EMCC) [9].

For the transducer free at both sides, the boundary conditions are established as the following:

$$\tilde{\tau} = 0 \quad \text{and} \quad \tilde{\phi} = 0 \qquad \text{at } z = 0, \tag{21a, b}$$

$$\tilde{\tau} = 0 \quad \text{and} \quad \tilde{\phi} = V_0 \qquad \text{at } z = l. \tag{21c, d}$$

Applying the boundary conditions (21) yields the following solutions:

$$\tilde{u}(z) = \frac{\varepsilon V_0}{\Delta_2} [\cos kz - \cos k(l - z)], \tag{22}$$

$$\tilde{\phi}(z) = \frac{V_0}{\Delta_2}\left\{\frac{\varepsilon^2}{\zeta} [\cos kz - \cos k(l - z) + \cos kl - 1] + \hat{G}k \sin klz\right\}, \tag{23}$$

$$\tilde{D} = -\frac{\zeta V_0}{\Delta_2} \hat{G}\ k \sin kl, \tag{24}$$

where

$$\Delta_2 \equiv \hat{G}kl \sin kl - 2\frac{\varepsilon^2}{\zeta}(1 - \cos kl) = 0 \quad (1 - \cos kl \neq 0) \tag{25}$$

is the characteristic equation representing the resonance of the single–disk torsional transducer free at both side surfaces. If $\cos kl = 1$, then $\tilde{u}(z) = 0$ and $\tilde{\phi}(z) = 0$, and the solutions are trivial.

3.2. Numerical results

The results of the analysis described in the previous section can be verified by calculating natural frequencies and comparing them with experimental observations. The piezoelectric material selected for the numerical calculation and experiment (in the next section) is PZT (EC65) made by EDO Co. The material properties are summarized in Table 1, and they are similar to the

Table 1
Electromechanical properties of a PZT (EDO EC-65)

Electromechanical properties	Values
Mass density, ρ	$7500\,\mathrm{kg/m^3}$
Permittivity, ζ	$8002\times10^{-12}\,\mathrm{C^2/N\,m^2}$
Piezoelectric strain constant, d_{15}	$584\times10^{-12}\,\mathrm{C/N}$
Elastic constant, s_{44}^E	$46.9\times10^{-12}\,\mathrm{m^2/N}$
Piezoelectric stress constant, $\varepsilon(=d_{15}/s_{44}^E)$	$12.45\,\mathrm{C/m^2}$
Shear modulus, $G(=1/s_{44}^E)$	21.3 GPa
Modified shear modulus, $\hat{G}(=G+\varepsilon^2/\zeta)$	40.7 GPa

Table 2
Natural frequencies of a single-disk transducer with fixed–free boundary conditions

Mode	Wavenumber × thickness			Natural frequency		
	Piezoelectric k_pl	Elastic k_el	k_pl-k_el	Piezoelectric f_p (kHz)	Elastic f_e (kHz)	f_p/f_e
1	1.19	1.57	−0.38	110	105	1.05
2	4.61	4.71	−0.10	427	316	1.35
3	7.79	7.85	−0.06	722	527	1.37
4	10.95	11.00	−0.05	1015	737	1.38

values reported in other literature [11]. The EMCC value of this material is 0.69. The thickness of this single–disk transducer is 4 mm.

The unknown variable k in Eqs. (20) and (25) can be calculated easily by using a root-finder function (FindRoot) available in Mathematica [12]. A successful search necessitates a good initial guess, which can be substituted by the elastic natural frequencies of a corresponding non-piezoelectric disk. Once the wavenumber k is evaluated, the natural frequency f is obtained from the following relation:

$$f=\frac{kc}{2\pi}. \tag{26}$$

For a transducer fixed at one side and free at the other side, the piezoelectric natural frequencies are calculated from Eqs. (20) and (26). The piezoelectric wavenumber k_p and the piezoelectric natural frequency f_p calculated for the first four modes are listed in Table 2. The wavenumbers in Table 2 are non-dimensional values normalized by multiplying the thickness of the transducer. The piezoelectric natural frequency calculated here will be compared with the measured one in the next section.

The elastic wavenumber k_e and the elastic natural frequency f_e of the non-piezoelectric disk are calculated to clarify the effect of the piezoelectric phenomenon on the natural frequency. This calculation is carried out by setting $\varepsilon=0$ and $\hat{G}=G$ in Eq. (20), and the results thus obtained are also listed in Table 2. The difference of the piezoelectric wavenumber and the elastic wavenumber k_p-k_e in Table 2 shows that the piezoelectric effect significantly reduces the wavenumber for the fundamental mode and the effect becomes trivial for the higher modes. This

Table 3
Natural frequencies of a single-disk transducer with free–free boundary conditions

Mode	Wavenumber × thickness			Natural frequency		
	Piezoelectric $k_p l$	Elastic $k_e l$	$k_p l - k_e l$	Piezoelectric f_p (kHz)	Elastic f_e (kHz)	f_p/f_e
0	—	0	—	—	0	—
1	2.38	3.14	−0.76	221	211	1.05
2	—	6.28	—	—	421	—
3	9.22	9.42	−0.20	854	632	1.35
4	—	12.57	—	—	843	—

is the same trend as appeared in the piezoelectric longitudinal transducer vibrating in the thickness direction [10]. The ratio of the corresponding natural frequencies f_p/f_e converge a typical value, $\sqrt{\hat{G}/G}$, for higher modes.

For the transducer free at both ends, the piezoelectric natural frequencies are calculated from Eqs. (25) and (26). The calculated piezoelectric wavenumbers and corresponding natural frequencies are listed in Table 3, and so are the elastic wavenumbers and corresponding natural frequencies. In this case, the piezoelectric resonance does not appear in the symmetric modes because of the constraint $\cos kl \neq 1$. The antisymmetric modes show the same trend as observed in Table 2.

The piezoelectric natural frequencies in Table 2 are a half of those frequencies in Table 3. This relation is explained in terms of mode shapes. The mode shapes of the single-disk transducer with fixed-free boundary conditions are calculated from Eq. (17) and displayed in Fig. 4. The mode shapes of the transducers with free–free boundary conditions are calculated from Eq. (22) and displayed in Fig. 5. In Figs. 4 and 5, the broken lines represent the mode shapes of the elastic resonance without piezoelectric phenomenon and the solid lines represent the mode shapes of the piezoelectric resonance.

It appears in Fig. 5 that the piezoelectric resonance of the free–free transducer does not have symmetric modes but has antisymmetric modes. The half of the antisymmetric mode shapes corresponds to the mode shapes in Fig. 4. Thus, the fixed–free transducer of half-thickness has the same piezoelectric resonance of the free–free transducer. Since the frequencies in Tables 2 and 3 are those of the transducers with the same thickness, the piezoelectric natural frequencies of fixed–free boundary conditions show twice the piezoelectric natural frequencies of free–free boundary conditions.

It is interesting to investigate the influence of geometrical parameter on the natural frequencies [13]. Fig. 6 shows the variation of the first natural frequency f_p with the thickness l of the piezoelectric disk calculated for fixed–free (broken line) and free–free (solid line) disks. It is obvious from the figure that the natural frequency is inversely proportional to the thickness of the disk.

3.3. Experiments

In order to verify the calculated values of the piezoelectric natural frequencies, measurements are carried out with the piezoelectric torsional transducers fabricated by the process illustrated in

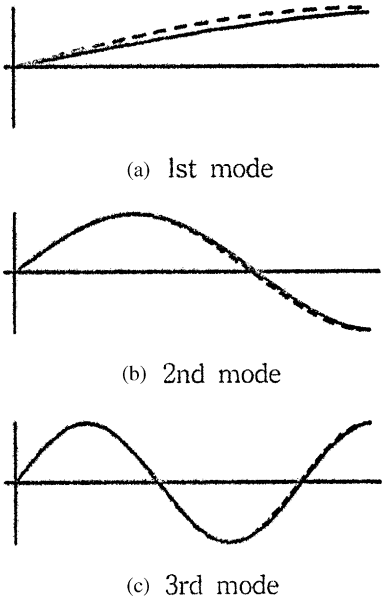

Fig. 4. Mode shapes of a single-disk transducer with fixed–free boundary conditions: (a) first, (b) second, and (c) third mode.

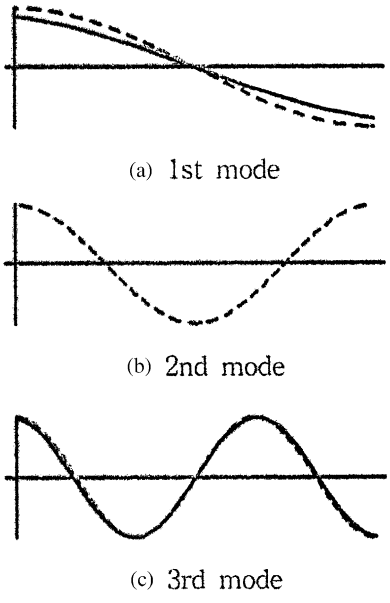

Fig. 5. Mode shapes of a single-disk transducer with free–free boundary conditions: (a) first, (b) second, and (c) third mode.

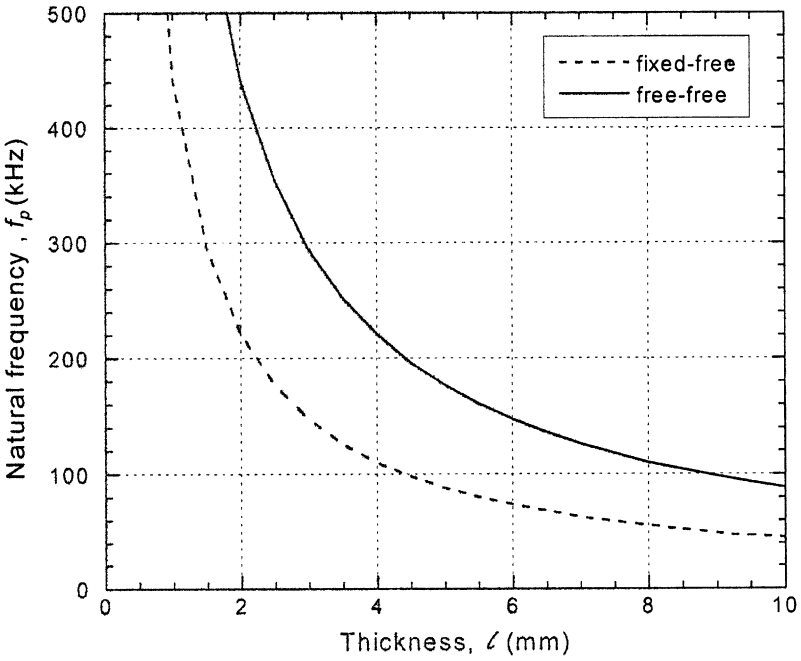

Fig. 6. Variation of the piezoelectric natural frequency f_p with the thickness l of the piezoelectric disk for the boundary conditions of fixed–free (broken line) and free–free (solid line).

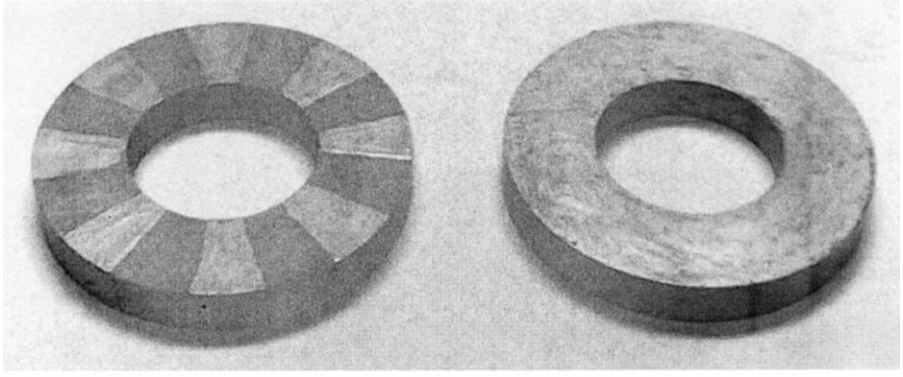

Fig. 7. Piezoelectric torsional transducer disks in the fabrication process: (a) covered with sector electrodes before polarization and (b) covered with whole electrodes after polarization.

Fig. 2. Fig. 7 shows the photograph of the transducer; (a) is the disk covered with sector electrodes before polarization and (b) is the disk covered with whole electrodes after polarization.

The resonance frequency of the transducer is measured by using impedance gain/phase analyzer (HP 4194A). The measured impedance displayed as a function of the frequency is shown in Fig. 8. The locations of local minimum impedance in the curve of Fig. 8 represent the piezoelectric

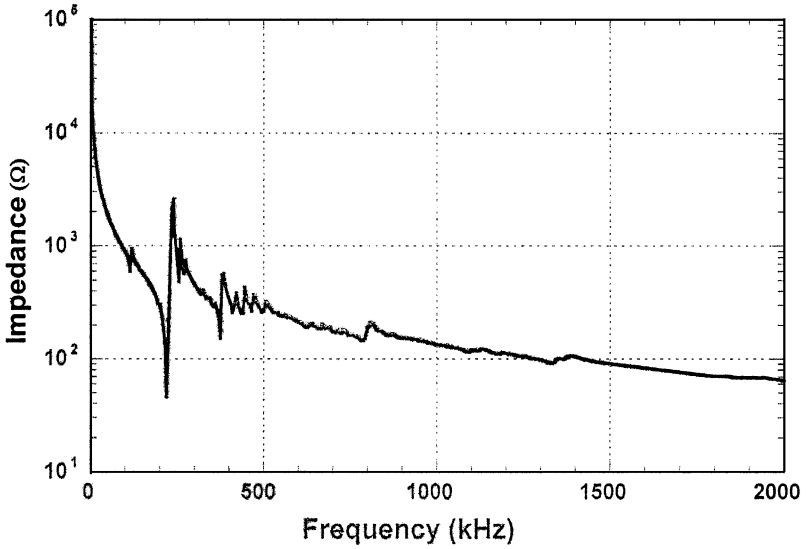

Fig. 8. Impedance curve of a single-disk transducer, measured as a function of the frequency.

Table 4
Comparison of the calculated and measured natural frequencies of a single-disk transducer with free–free boundary conditions

Mode	Natural frequency (kHz)		Difference (%)
	Calculated	Measured	
1	221	225	−1.8
2	854	805	6.1
3	1445	1380	4.7
4	2030	1940	4.6

natural frequencies. The measured piezoelectric natural frequencies are listed in Table 4 and compared to the calculated ones. The calculated and measured values agree with each other.

4. Vibration of double-disk transducers

The analysis for the single-disk transducer described in the previous section is extended to the case of the double-disk transducer which is the realistic part of the BLT considered in the next section.

4.1. Analysis

The double-disk transducer consists of two piezoelectric torsional disks, 1 and 2 in Fig. 9, of the thickness l and polarized in the opposite directions. The transducer is driven by the electric

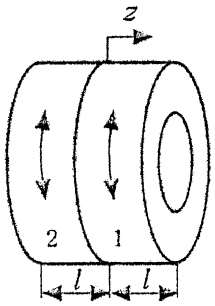

Fig. 9. Schematic diagram of a double-disk transducer.

voltage $V_0 e^{j\omega t}$ applied to the side surface of each disk. Thus, the driving voltage can be regarded as the voltage $V_0 e^{j\omega t}$ on the outer surface and voltage 0 on the inner surface. Mechanically, the outer surfaces are free, and the boundary conditions are established as follows:

$$\tilde{u}_1 = \tilde{u}_2, \quad \tilde{\tau}_1 = \tilde{\tau}_2, \quad \tilde{\phi}_1 = 0, \quad \tilde{\phi}_2 = 0, \quad \text{at } z = 0, \tag{27a, b, c, d}$$

$$\tilde{\tau}_1 = 0, \quad \tilde{\phi}_1 = V_0 \quad \text{at } z = l, \tag{27e, f}$$

$$\tilde{\tau}_2 = 0, \quad \tilde{\phi}_1 = V_0 \quad \text{at } z = -l, \tag{27g, h}$$

Subscripts 1 and 2 represent the corresponding piezoelectric disks. The governing equation (16) is replaced by the following one for disk 2 because of the opposite direction of polarization:

$$\frac{d^2\tilde{\phi}}{dz^2} = -\frac{\varepsilon}{\zeta}\frac{d^2\tilde{u}}{dz^2}. \tag{28}$$

Applying the boundary conditions (27a–27 h) yields the following solutions:

$$\tilde{u}_1(z) = \frac{\varepsilon V_0}{\Delta_1}\sin kz, \tag{29}$$

$$\tilde{\phi}_1(z) = \frac{V_0}{\Delta_1}\left[\frac{\varepsilon^2}{\zeta}\sin kz - (\hat{G}k\cos kl)z\right], \tag{30}$$

$$\tilde{D}_1 = \frac{\zeta V_0}{\Delta_1}\hat{G}k\cos kl, \tag{31}$$

$$\tilde{u}_2(z) = \frac{\varepsilon V_0}{\Delta_1}\sin kz, \tag{32}$$

$$\tilde{\phi}_2(z) = -\frac{V_0}{\Delta_1}\left[\frac{\varepsilon^2}{\zeta}\sin kz - (\hat{G}k\cos kl)z\right], \tag{33}$$

$$\tilde{D}_2 = \frac{\zeta V_0}{\Delta_1}\hat{G}k\cos kl. \tag{34}$$

It appears that the characteristic equation representing the resonance of the double–disk transducer free at both outer surfaces is again Eq. (20), which is the characteristic equation for the

Table 5
Natural frequencies of a double-disk transducer and a symmetric Langevin-type double-disk transducer, both with free–free boundary conditions

Mode	Piezoelectric natural frequency		
	Two-layer, f_p (kHz)	Langevin-type two-layer, f_L (kHz)	f_L/f_p
1	110	22.4	0.20
2	427	65.7	0.15
3	722	107	0.15
4	1015	148	0.15

single–disk transducer fixed at one side and free at the other. Therefore, the piezoelectric natural frequencies of the symmetric double–disk transducer can also be calculated by the analysis for the symmetric half.

4.2. Numerical results

Since the piezoelectric natural frequencies of the double–disk transducer are calculated with Eq. (20), the numerical results listed in Table 2 are also valid and used as the frequency f_p in Table 5. These results are compared with those of the Langevin–type transducers in the next section.

It is interesting to note that the natural modes of the double-disk transducer, Eqs. (28)–(33), are the same equations (17)–(19) as those of the single–disk transducer with fixed–free boundary conditions, and that the fixed–free transducer has the same piezoelectric resonance as the free–free transducer of double thickness. In other words, the symmetric double-disk transducer can be regarded as a single-disk transducer as if there is no interface between the two disks. The voltage between two surfaces is regarded as $2V_0 e^{j\omega t}$ this consideration.

5. Vibration of the Langevin-type torsional transducers

The double-disk torsional transducers described in the previous section are assembled together with two elastic blocks to form a torsional BLT as shown in Fig. 1. If two elastic blocks are the same, the BLT is then regarded as a symmetric one. Otherwise, the BLT is asymmetric.

5.1. Analysis and numerical results for symmetric BLT's

A symmetric BLT shown in Fig. 10(a) is a special case of the transducer shown in Fig. 1 in that the elastic blocks A and B are identical. Piezoelectric torsional disks 1 and 2 of thickness l_1 are coupled and elastic blocks A and B of thickness l_2 are assembled at each side. A full analysis with the boundary conditions at two boundaries and three interfaces would be complicated. Thus, based on the discussions in the previous section, the analysis is carried out for the symmetric half shown in Fig. 10(b).

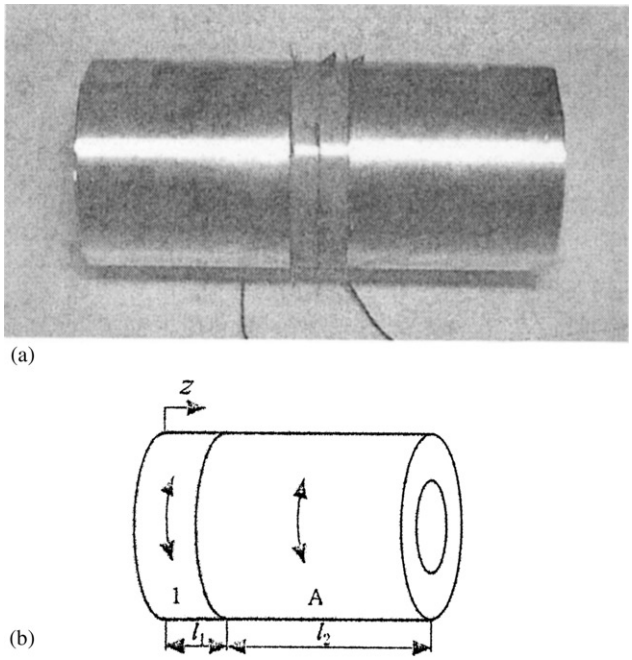

Fig. 10. Symmetric Langevin-type transducer: (a) photo, (b) schematic diagram of the symmetric half.

The symmetry face is regarded as a fixed one, and the boundary and interface conditions are established as follows when the piezoelectric disk is driven by the voltage $V_0 e^{j\omega t}$.

$$\tilde{u}_1 = 0 \quad \text{and} \quad \tilde{\phi}_1 = 0 \quad \text{at } z = 0, \tag{35a, b}$$

$$\tilde{u}_1 = \tilde{u}_A, \quad \tilde{\tau}_1 = \tilde{\tau}_A, \quad \text{and} \quad \tilde{\phi}_1 = V_0 \quad \text{at } z = l, \tag{35c, d, e}$$

$$\tilde{\tau}_A = 0 \quad \text{at } z = l_1 + l_2. \tag{35f}$$

The governing equations for the piezoelectric disk are the same as Eqs. (9) and (10). The equation for the elastic blocks is the same as Eq. (9) with $\varepsilon = 0$.

Applying the boundary conditions (35a–35f) yields the solutions for the symmetric torsional BLT as follows:

$$\tilde{u}_1(z) = \frac{\varepsilon V_0}{\Delta_3} \frac{\cos k_2 l_2}{\sin k_1 l_1} \sin k_1 z, \tag{36}$$

$$\tilde{\phi}_1(z) = \frac{1}{\Delta_3} \frac{\varepsilon^2 V_0}{\zeta} \frac{\cos k_2 l_2}{\sin k_1 l_1} \sin k_1 z - \left(\frac{1}{\Delta_3} \frac{\varepsilon^2 V_0}{\zeta} \cos k_2 l_2 + \frac{V_0}{l_1} \right) z, \tag{37}$$

$$\tilde{D}_1 = \frac{1}{\Delta_3} \varepsilon^2 V_0 \cos k_2 l_2 + \frac{\zeta V_0}{l_1}, \tag{38}$$

$$\tilde{u}_A(z) = \frac{\varepsilon V_0}{\Delta_3} \cos k_2 (l_1 + l_2 - z), \tag{39}$$

Table 6
Elastic properties of aluminum alloy (2014-T6) and stainless steel (STS-302)

	Properties	Values
2014-T6	Mass density, ρ	2800 kg/m^3
	Shear modules, G	28 GPa
STS-302	Mass density, ρ	7920 kg/m^3
	Shear modules, G	75 GPa

Table 7
Comparison of the calculated and measured natural frequencies of a symmetric Langevin-type transducer

Mode	Natural frequency (kHz)		Difference (%)
	Calculated	Measured	
1	22.4	19.8	13
2	65.7	58.2	13
3	107	90.7	18
4	148	161	–8

where

$$\Delta_3 \equiv \left(\frac{\varepsilon^2}{\zeta}\sin k_1 l_1 - \hat{G}_1 k_1 l_1 \cos k_1 l_1\right)\cos k_A l_2 + C_A k_A l_1 \sin k_1 l_1 \sin k_A l_2 = 0 \tag{40}$$

is the characteristic equation representing the resonance of the symmetric torsional BLT.

If the elastic blocks A and B do not exist, Eq. (40) becomes the same as Eq. (20). This degradation is consistent with the statement discussed for the double–disk transducer in the previous section.

The piezoelectric natural frequencies of the symmetric torsional BLT are calculated from Eq. (40). The piezoelectric disk is the same as those mentioned in the previous sections, and the material properties and thickness are the same as those used earlier. The elastic blocks are made of aluminum alloy (2014-T6) and the material properties [14] are listed in Table 6. The natural frequencies have been calculated and listed in Tables 5 and 7 according to the procedure of numerical calculation described in Section 3.2

Table 5 compares the natural frequencies of the double–disk transducer and the Langevin-type transducer including the double disks. It appears that the piezoelectric natural frequencies of the BLT are about 15–20% of those of the double–disk transducer due to the elastic blocks which are 7.5 times thicker than the disk. Table 7 compares the calculated frequencies with the measured ones.

Usually, the natural frequency of piezoelectric disks is higher than desired. Increasing the disk thickness to reduce the natural frequency results in the loss of the electromechanical efficiency. Thus, attaching the elastic blocks is the best way to reduce the natural frequency of the piezoelectric transducer. The thickness of the elastic block can be selected to make the desired natural frequency by the analysis shown in this section.

The mode shapes corresponding to the natural frequencies are calculated from Eqs. (36) and (39), and displayed in Fig. 11. The shape of the one-half is the duplication of the calculated results

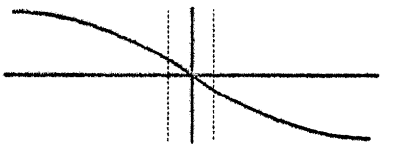

(a) 1st mode (22.4 kHz)

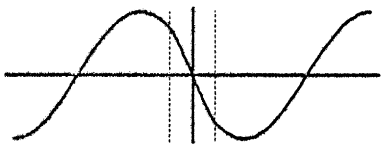

(b) 2nd mode (65.7 kHz)

Fig. 11. Mode shapes of the symmetric Langevin-type transducer: (a) first mode (22.4 kHz), (b) second mode (65.7 kHz).

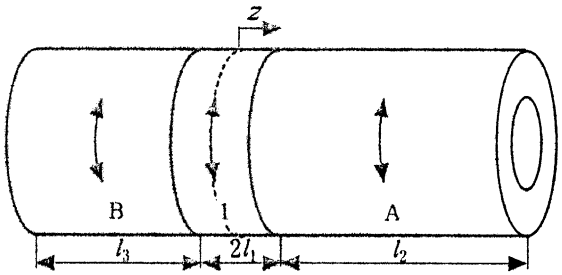

Fig. 12. Schematic diagram of the asymmetric Langevin-type transducer.

for the other half so that the mode shape becomes antisymmetric. The dotted lines represent the interface between the piezoelectric layers and the elastic blocks.

5.2. *Analysis and numerical results for asymmetric BLT's*

Two elastic blocks in a BLT are in general not identical, and the transducer is asymmetric, as shown in Fig. 1. The asymmetric BLT consists of piezoelectric disks 1 and 2 of thickness l_1, as shown in Fig. 9, and elastic blocks A and B of thickness l_2 and l_3, respectively, as shown in Fig. 12. Based on the discussion in Section 4.2, the piezoelectric disks 1 and 2 are considered as a single piezoelectric disk of thickness $2l_1$ to simplify the analysis.

When the piezoelectric disk is derived by the voltage $2V_0 e^{j\omega t}$, the boundary and interface conditions are established as follows:

$$\tilde{u}_1 = \tilde{u}_A, \quad \tilde{\tau}_1 = \tilde{\tau}_A, \quad \tilde{\phi}_1 = 2V_0 \quad \text{at } z = l_1, \tag{41a,b,c}$$

$$\tilde{u}_1 = \tilde{u}_B, \quad \tilde{\tau}_1 = \tilde{\tau}_B, \quad \tilde{\phi}_1 = 0 \quad \text{at } z = -l_1, \tag{41d,e,f}$$

$$\tilde{\tau}_A = 0 \quad \text{at } z = l_1 + l_2, \tag{41g}$$

$$\tilde{\tau}_B = 0 \quad \text{at } z = -(l_1 + l_3). \tag{41h}$$

Using the governing equations from Section 5.1 and applying the boundary conditions (41a)–(41 h) yields the solutions for the asymmetric torsional BLT as follows:

$$\tilde{u}_1(z) = A_1 \cos k_1 z + B_1 \sin k_1 z, \tag{42}$$

$$\begin{aligned} A_1 &= -\frac{\varepsilon V_0}{\Delta_4}\left[G_A k_A l_1 \sin k_A l_2 \cos k_B l_3 - G_B k_B l_1 \cos k_A l_2 \sin k_B l_3\right] \sin k_1 l_1, \\ B_1 &= \frac{\varepsilon V_0}{\Delta_4}\left[2\hat{G}_1 k_1 l_1 \sin k_1 l_1 \cos k_A l_2 \cos k_B l_3\right. \\ &\quad \left. + G_A k_A l_1 \cos k_1 l_1 \sin k_A l_2 \cos k_B l_3 + G_B k_B l_1 \cos k_1 l_1 \cos k_A l_2 \sin k_B l_3\right], \end{aligned}$$

$$\tilde{\phi}_1(z) = \frac{\varepsilon}{\zeta}\tilde{u}_1(z) + az + b, \tag{43}$$

$$\begin{aligned} a &= -\frac{1}{l_1}\left(\frac{\varepsilon}{\zeta}\sin k_1 l_1 B_1 - V_0\right), \\ b &= -\frac{\varepsilon}{\zeta}(\cos k_1 l_1 A_1 - \sin k_1 l_1 B_1) + l_1 a, \end{aligned}$$

$$\tilde{u}_A(z) = A_2 \cos k_A z + B_2 \sin k_A z, \tag{44}$$

$$\begin{aligned} A_2 &= \frac{2\varepsilon V_0}{\Delta_4}\left(\hat{G}_1 k_1 l_1 \sin k_1 l_1 \cos k_B l_3 + G_B k_B l_1 \cos k_1 l_1 \sin k_B l_3\right) \sin k_1 l_1 \cos k_A (l_1 + l_2), \\ B_3 &= \frac{2\varepsilon V_0}{\Delta_4}\left(\hat{G}_1 k_1 l_1 \sin k_1 l_1 \cos k_B l_3 + G_B k_B l_1 \cos k_1 l_1 \sin k_B l_3\right) \sin k_1 l_1 \sin k_A (l_1 + l_2), \end{aligned}$$

$$\tilde{u}_B(z) = A_3 \cos k_B z + B_3 \sin k_B z, \tag{45}$$

$$\begin{aligned} A_3 &= -\frac{2\varepsilon V_0}{\Delta_4}\left(\hat{G}_1 k_1 l_1 \sin k_1 l_1 \cos k_A l_2 + G_A k_A l_1 \cos k_1 l_1 \sin k_A l_2\right) \sin k_1 l_1 \cos k_B (l_1 + l_3), \\ B_3 &= -\frac{2\varepsilon V_0}{\Delta_4}\left(\hat{G}_1 k_1 l_1 \sin k_1 l_1 \cos k_A l_2 + G_A k_A l_1 \cos k_1 l_1 \sin k_A l_2\right) \sin k_1 l_1 \sin k_B (l_1 + l_3), \end{aligned}$$

where

$$\begin{aligned} \Delta_4 \equiv{}& \left[\hat{G}_1 k_1 l_1 \sin k_1 l_1 \cos k_A l_2 + G_A k_A l_1 \cos k_1 l_1 \sin k_A l_2\right] \\ &\times \left[\left(\frac{\varepsilon^2}{\zeta}\sin k_1 l_1 - \hat{G}_1 k_1 l_1 \cos k_1 l_1\right)\cos k_B l_3 + G_B k_B l_1 \sin k_1 l_1 \sin k_B l_3\right] \\ &+ \left[\hat{G}_1 k_1 l_1 \sin k_1 l_1 \cos k_B l_3 + G_B k_B l_1 \cos k_1 l_1 \sin k_B l_3\right] \\ &\times \left[\left(\frac{\varepsilon^2}{\zeta}\sin k_1 l_1 - \hat{G}_1 k_1 l_1 \cos k_1 l_1\right)\cos k_A l_2 + G_A k_A l_1 \sin k_1 l_1 \sin k_A l_2\right] \\ ={}& 0 \end{aligned} \tag{46}$$

is the characteristic equation representing the resonance of the asymmetric torsional BLT. If $G_A = G_B$, $k_A = k_B$, and $l_2 = l_3$, then Eqs. (42)–(46) become Eqs. (36)–(40), which are the solutions for the symmetric BLT.

Table 8
Comparison of the calculated and measured natural frequencies of an asymmetric Langevin-type transducer

Mode	Natural frequency (kHz)		Difference (%)
	Calculated	Measured	
1	15.4	13.7	12
2	30.3	27.7	9
3	44.1	40.9	8
4	61.8	56.0	10

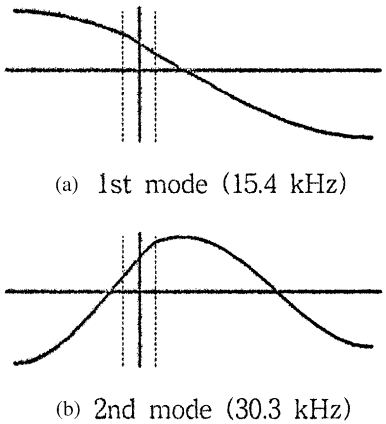

Fig. 13. Mode shapes of the asymmetric Langevin-type transducer with different block size: (a) first mode (15.4 kHz), (b) second mode (30.3 kHz).

With the same material properties mentioned in Section 5.1 except that the thickness of the elastic block A is 60 mm, the piezoelectric natural frequencies of the asymmetric BLT have been calculated from Eq. (46). The calculated frequencies are listed in Table 8 and will be compared with the measured ones in the next section. The mode shapes corresponding to the natural frequencies are calculated from Eqs. (42), (44), and (45) and displayed in Fig. 13.

On the other hand, an asymmetric BLT with the elastic blocks of the same size, 30 mm thickness, but different materials, for example stainless steel (STS-302) for A and aluminum alloy (2014-T6) for B, can also be considered. The material properties of stainless steel [15] together with the properties of aluminium alloy are listed in Table 6. The natural frequencies and mode shapes are calculated and shown in Fig. 14.

Figs. 13(a) and 14(a) represent the 1st mode and show the shapes similar to the antisymmetric mode of Fig. 11(a) even though the location of the nodal point is not symmetric. Figs. 13(b) and 14(b) represent the 2nd mode and show the shapes corresponding to the symmetric mode which does not appear in a symmetric transducer, but the location of the nodal point is of course not symmetric. As shown in Figs. 13 and 14, the asymmetric BLT possesses both antisymmetric and symmetric modes and asymmetric nodal position.

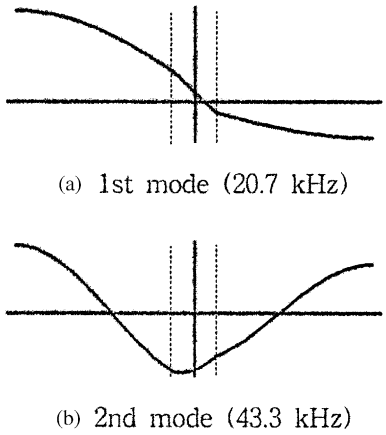

Fig. 14. Mode shapes of the asymmetric Langevin-type transducer with different block material: (a) first mode (20.7 kHz), (b) second mode (43.3 kHz).

5.3. Experiments

In order to verify the analysis for the vibration of the Langevin-type torsional transducers, the piezoelectric natural frequencies are measured for comparison with the calculated ones. The transducers used for the experiment are the symmetric BLT shown in Fig. 10(a) and the asymmetric one in Fig. 1(a).

The piezoelectric natural frequencies of the BLT are measured by the procedure described in Section 3.3 The measured impedance curves are shown in Fig. 15(a) and (b). The measured natural frequencies, which is the location of the local minimum in the impedance curve, are listed in Tables 7 and 8, and compared with the calculated ones. The 10% difference between the measured and calculated values seems due to the factors insufficiently considered in the analysis model. Such factors include the steel bolt clamping the elastic blocks and the flat cut of one portion of the elastic blocks. If the error due to the difference of the models is accepted, the analysis results are reasonable.

6. Conclusion

The vibrational characteristics of piezoelectric torsional transducers of single-disk and double-disk and Langevin-type piezoelectric torsional transducers were studied by deriving the characteristic equations and vibration modes. The piezoelectric natural frequencies of the transducers were calculated from the theoretical solutions and then compared with measured values. The comparison verifies that the theoretical results are reasonable.

The analysis for the single-disk transducer shows that the piezoelectric resonance of the free–free boundary conditions does not have symmetric modes but has antisymmetric modes. A fixed–free transducer of half-thickness has the same piezoelectric resonance of a free–free transducer.

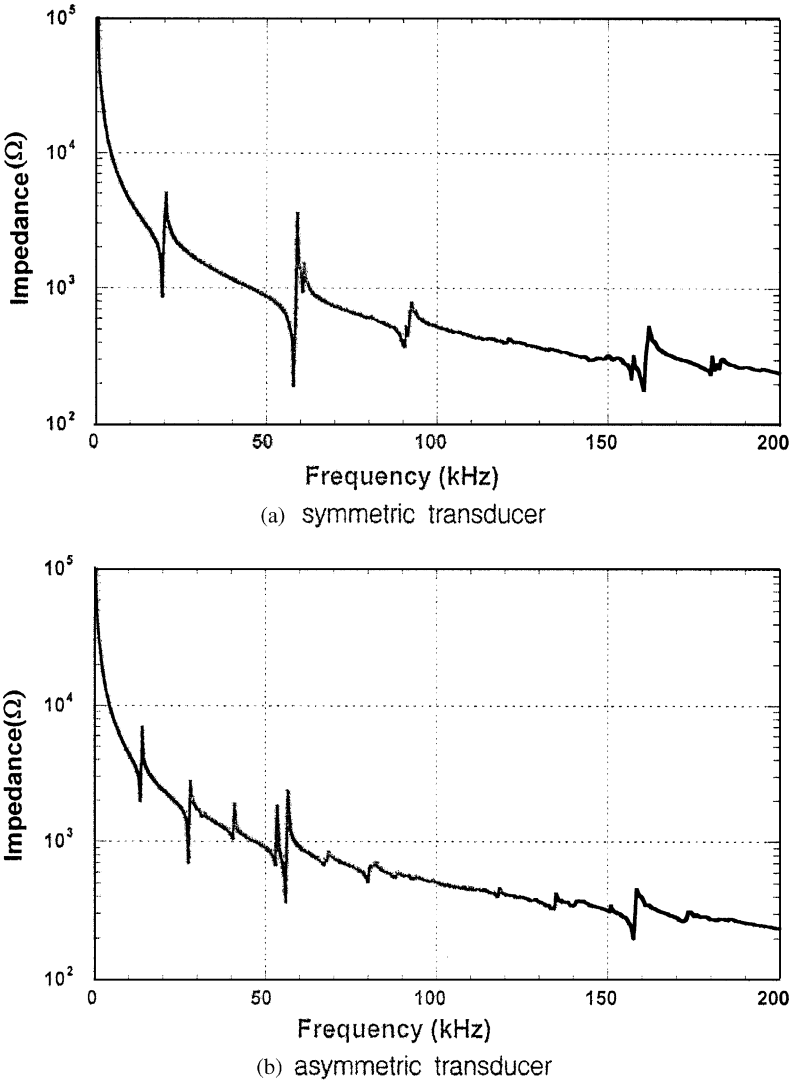

Fig. 15. Impedance curves of Langevin-type transducers, measured as a function of the frequency: (a) symmetric transducer, (b) asymmetric transducer.

A symmetric transducer with two identical elastic blocks has symmetric modes only and the analysis can be carried out for the symmetric half of the transducer. General cases of asymmetric transducers were considered for the transducer with two elastic blocks of the same material but different size and for the transducer with two elastic blocks of the same size but different materials. The asymmetric transducers have mode shapes corresponding to the symmetric and antisymmetric modes.

The theoretically derived characteristic equations enable one to quantitatively predict the effect of the elastic blocks on the reduction of the natural frequencies of a Langevin-type torsional

transducer. The results establish the design base of the transducer with desired natural frequencies by adequately selecting the size of the elastic blocks of the transducer.

Acknowledgements

This work was supported by ISTEC Co., Ltd. with a grant from the Korean Ministry of Commerce, Industry and Energy.

References

[1] T. Ikeda, Fundamentals of Piezoelectricity, Oxford University Press, Oxford, 1996.
[2] K. Uchino, Piezoelectric Actuators and Ultrasonic Motors, Kluwer Academic Publisher, Boston, 1997.
[3] T. Sashida, T. Kenjo, An Introduction to Ultrasonic Motors, Oxford University Press, Oxford, 1993.
[4] J.O. Kim, Y. Wang, H.H. Bau, The effect of an adjacent viscous fluid on the transmission of torsional stress waves in a submerged waveguide, Journal of the Acoustical Society of America 89 (3) (1991) 1414–1422.
[5] J.O. Kim, Torsional wave propagation in a circular cylinder with a periodically corrugated outer surface, American Society of Mechanical Engineers, Journal of Vibration and Acoustics 121 (4) (1999) 501–505.
[6] S. Mishiro, Torsional vibration apparatus, United States Patent 4,652,786, 1987.
[7] S. Mishiro, Torsion vibrator, United States Patent 4,787,265, 1988.
[8] S. Nemoto, E. Mori, Bolt-clamped electrostrictive torsional vibrator (in Japanese), Journal of the Acoustical Society of Japan 28 (3) (1972) 117–126.
[9] S. Lin, Study of the sandwiched piezoelectric ultrasonic torsional transducer, Ultrasonics 32 (6) (1994) 461–465.
[10] D.K. Miu, Mechatronics: Electromechanics and Contromechanics, Springer, New York, 1993 (Chapter 6).
[11] D.A. Berlincourt, C. Cmolik, H. Jaffe, Piezoelectric properties of polycrystalline lead titanate zirconate compositions, Proceedings of the IRE, 1960, pp. 220–229.
[12] S. Wolfram, Mathematica: A System for Doing Mathematics by Computer, Addison-Wesley, New York, 1988.
[13] P. Lu, K.H. Lee, W.Z. Lin, F. Shen, S.P. Lim, An approximate frequency formula for piezoelectric circular cylindrical shells, Journal of Sound and Vibration 242 (2001) 309–320.
[14] J.M. Gere, S.P. Timoshenko, Mechanics of Materials, 3rd Edition, PWS, Warsaw, 1990, pp. 777–782.
[15] F.P. Beer, E.R. Johnston, Mechanics of Materials, 2nd Edition in SI Units, Appendix B, McGraw-Hill, New York, 1992.